Published in Chemistry - A European Journal, 10, issue 1, 208-217, 2003
which should be used for any reference to this work

Framework Fluxionality of Organometallic Oxides: Synthesis, Crystal Structure, EXAFS, and DFT Studies on [{Ru(η^6-arene)}$_4$Mo$_4$O$_{16}$] Complexes

Danielle Laurencin,[a] Eva Garcia Fidalgo,[b] Richard Villanneau,[a] Françoise Villain,[a, c] Patrick Herson,[a] Jessica Pacifico,[b] Helen Stoeckli-Evans,[b] Marc Bénard,[d] Marie-Madeleine Rohmer,[d] Georg Süss-Fink,[b] and Anna Proust*[a]

Dedicated to Professor Pierre Gouzerh on the occasion of his 60th birthday

Abstract: Reactions of the molybdates $Na_2MoO_4{\cdot}2H_2O$ and $(n\mathrm{Bu_4N})_2[Mo_2O_7]$ with [{Ru(arene)Cl$_2$}$_2$] (arene = $C_6H_5CH_3$, 1,3,5-$C_6H_3(CH_3)_3$, 1,2,4,5-$C_6H_2(CH_3)_4$) in water or organic solvents led to formation of the triple-cubane organometallic oxides [{Ru(η^6-arene)}$_4$Mo$_4$O$_{16}$], whose crystal and molecular structures were determined. Refluxing triple cubane [{Ru(η^6-$C_6H_5CH_3$)}$_4$Mo$_4$O$_{16}$] in methanol caused partial isomerization to the windmill form. The two isomers of [{Ru(η^6-$C_6H_5CH_3$)}$_4$Mo$_4$O$_{16}$] were characterized by Raman and Mo K-edge X-ray absorption spectroscopy (XAS), both in the solid-state and in solution. This triple-cubane isomer was also used as a spectroscopic model to account for isomerization of the *p*-cymene windmill [{Ru(η^6-1,4-$CH_3C_6H_4CH(CH_3)_2$)}$_4$Mo$_4$O$_{16}$] in solution. Using both Raman and XAS techniques, we were then able to determine the ratio between the windmill and triple-cubane isomers in dichloromethane and in chloroform. Density functional calculations on [{Ru(η^6-arene)}$_4$Mo$_4$O$_{16}$] (arene = C_6H_6, $C_6H_5CH_3$, 1,3,5-$C_6H_3(CH_3)_3$, 1,4-$CH_3C_6H_4CH(CH_3)_2$, $C_6(CH_3)_6$) suggest that the windmill form is intrinsically more stable, provided the complexes are assumed to be isolated. Intramolecular electrostatic interactions and steric bulk induced by substituted arenes were found to modulate but not to reverse the energy difference between the isomers. The stability of the triple-cubane isomers should therefore be accounted for by effects of the surroundings that induce a shift in the energy balance between both forms.

Keywords: density functional calculations · EXAFS spectroscopy fluxionality · organo-metallic oxides polyoxometalates

Introduction

Stoichiometric or catalytic transformations of organic substrates by ruthenium complexes, and especially by {Ru(arene)}$^{2+}$-containing species, are now well documented. Compounds of this type are active catalysts in a growing number of reactions, which include hydrogenation,[1] oxidation,[2] C–C coupling (including olefin metathesis),[3] and nucleophilic addition to multiple bonds.[4] In fact, the impact of ruthenium in organic synthesis has now attained that of palladium.[5] This extensive reactivity is associated with the exceptional properties of ruthenium: 1) it has the widest scope of oxidation states of all elements (from $-$II to $+$VIII), 2) a large number of coordination geometries are known for ruthenium complexes, and 3) it can be surrounded by hard ($\sigma+\pi$) donor ligands (e.g., oxo ligands as in [$Ru^{VIII}O_4$]) or by soft σ-donor/π-acceptor ligands (e.g., carbonyl ligands as in [$Ru^{-II}(CO)_4]^{2-}$). Hence, ruthenium is particularly suited for the design of organometallic oxo complexes, at the interface of classical coordination chemistry and organometallic

[a] D. Laurencin, Dr. R. Villanneau, Dr. F. Villain, P. Herson, Prof. A. Proust
Laboratoire de Chimie Inorganique et Matériaux Moléculaires
UMR CNRS 7071, Université Pierre et Marie Curie
case courrier 42, 4 Place Jussieu, 75252 Paris Cedex 05 (France)
Fax: (+33) 1-4427-3841
E-mail: proust@ccr.jussieu.fr

[b] Dr. E. Garcia Fidalgo, Dr. J. Pacifico, Prof. H. Stoeckli-Evans, Prof. G. Süss-Fink
Institut de Chimie, Université de Neuchâtel
case postale 2, CH-2000 Neuchâtel (Switzerland)

[c] Dr. F. Villain
Laboratoire d'Utilisation du Rayonnement Electromagnétique
Batiment 209d, Centre Universitaire Paris-Sud
BP 34, 91898 Orsay Cedex (France)

[d] Dr. M. Bénard, Dr. M.-M. Rohmer
Laboratoire de Chimie Quantique, UMR CNRS 7551
Université Louis Pasteur, 4 rue Blaise Pascal, 67000 Strasbourg (France)

chemistry. Although $\{Ru(arene)\}^{2+}$ derivatives of polyoxometalates have been known for almost fifteen years,[6] this field has experienced growing interest after the report of the windmill-like structure of the *p*-cymene complex $[\{Ru(\eta^6\text{-}1,4\text{-}CH_3C_6H_4CH(CH_3)_2)\}_4Mo_4O_{16}]$.[7] Since then, more than a dozen arene Ru oxo complexes with various nuclearities and structures have been reported.[8,9] With respect to their catalytic potential, particular attention was paid to the framework fluxionality of these complexes in solution. Indeed, $[\{Ru(\eta^6\text{-}1,4\text{-}CH_3C_6H_4\text{-}CH(CH_3)_2)\}_4Mo_4O_{16}]$ was proposed to isomerize into its triple-cubane isomer (Scheme 1)

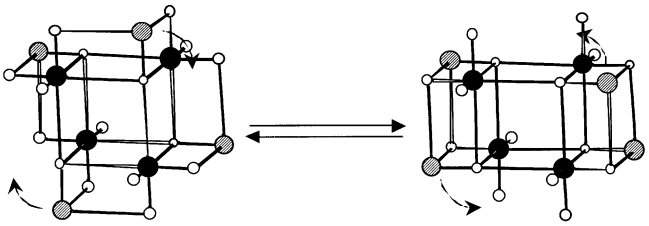

Scheme 1.

on dissolution in chlorinated solvents, as suggested by multinuclear NMR techniques.[9a] By varying the arene ligands (hexamethylbenzene instead of *p*-cymene) and/or the metal (tungsten instead of molybdenum), it was possible to favour the windmill-like isomers, which have been characterized both in solution and in the solid state.[9a,b] In the present work, the influence of less bulky arenes such as toluene, mesitylene and durene on the formation of $[\{Ru(\eta^6\text{-arene})\}_4Mo_4O_{16}]$ complexes and their isomerization is addressed. Here we report on the synthesis and structural characterization of $[\{Ru(\eta^6\text{-}C_6H_5CH_3)\}_4Mo_4O_{16}]$, $[\{Ru(\eta^6\text{-}1,3,5\text{-}C_6H_3(CH_3)_3\}_4Mo_4O_{16}]$ and $[\{Ru(\eta^6\text{-}1,2,4,5\text{-}C_6H_2(CH_3)_4\}_4Mo_4O_{16}]$, and on studies on the framework isomerization of $[\{Ru(\eta^6\text{-}C_6H_5CH_3)\}_4Mo_4O_{16}]$ and $[\{Ru(\eta^6\text{-}1,4\text{-}CH_3C_6H_4CH(CH_3)_2)\}_4Mo_4O_{16}]$ in solution by Raman and X-ray absorption techniques. Density functional geometry optimizations were carried out on the two isomers of $[\{Ru(\eta^6\text{-arene})\}_4Mo_4O_{16}]$ for a variety of arene ligands, including benzene, to clarify the influence of steric crowding and electrostatic interactions of the ligand framework on the relative stabilities of the two isomers.

Results and Discussion

Syntheses: We previously reported the reactions of the molybdates $Na_2MoO_4{\cdot}2H_2O$ and $(nBu_4N)_2[Mo_2O_7]$ with $[\{Ru(arene)Cl_2\}_2]$ (arene = *p*-cymene, hexamethylbenzene).[8,9] In an attempt to rationalize the effect of various arene ligands on the formation of $\{Ru(arene)\}^{2+}$-containing organometallic oxides, we studied the reactivity of the less bulky toluene, mesitylene and durene analogues. This study also included the parent benzene complex $[\{Ru(\eta^6\text{-}C_6H_6)Cl_2\}_2]$; however, due to their insolubility, none of the products formed in this case could be properly characterized, with the exception of the tetranuclear methoxo complex $[\{Ru(\eta^6\text{-}C_6H_6)\}_2Mo_2O_6(OMe)_4]$, the structure of which is derived from that of $[Mo_4O_{10}(OMe)_6]^{2-}$.[10]

The triple-cubane complexes **1a**, **2a** and **3a** were obtained in water from the reaction of $Na_2MoO_4{\cdot}2H_2O$ with $[\{Ru(\eta^6\text{-}C_6H_5CH_3)Cl_2\}_2]$, $[\{Ru(\eta^6\text{-}1,3,5\text{-}C_6H_3(CH_3)_3)Cl_2\}_2]$ and $[\{Ru(\eta^6\text{-}1,2,4,5\text{-}C_6H_2(CH_3)_4)Cl_2\}_2]$, respectively, in a 1/1 Mo/Ru ratio for **1a** and **2a** and a 5/1 Mo/Ru ratio for **3a** (method 1). Increasing the Mo/Ru ratio in the synthesis of **1a** and **2a** did not improve the yield, which never exceeded 50%. These preparations were adapted from that of the *p*-cymene complex **4b**, which has a windmill-like structure in the solid state but is proposed to isomerize into its triple-cubane isomer **4a** in solution.[7] The windmill complex **5b** was similarly obtained from $[\{Ru(\eta^6\text{-}C_6Me_6)Cl_2\}_2]$ but together with $[\{Ru(\eta^6\text{-}C_6Me_6)\}_2Mo_5O_{18}\{Ru(\eta^6\text{-}C_6Me_6)(H_2O)\}]$.[9b] Both **1a** and **2a** could also be obtained in acetonitrile solution by reaction of $(nBu_4N)_2[Mo_2O_7]$ and the corresponding $[\{Ru(arene)Cl_2\}_2]$ complex (method 2). Furthermore, **2a** was also obtained from the reaction of $(nBu_4N)_2[Mo_2O_7]$ with $[Ru(\eta^6\text{-}C_6H_3(CH_3)_3)Cl_2]_2$ in methanol at a Mo/Ru ratio of 2/1 (method 3). Refluxing a suspension of **1a** in methanol for 2 h led to formation of the windmill isomer **1b**. However, the isomerization of **1a** to **1b** was incomplete, even when heating was prolonged to almost 12 h, and led to a mixture of the isomers in the solid state, as far as can be judged from the IR and Mo K-edge EXAFS spectra.

Triple-cubane isomers:

$[\{Ru(\eta^6\text{-}C_6H_5CH_3)\}_4Mo_4O_{16}]$ **1a**

$[\{Ru(\eta^6\text{-}C_6H_3(CH_3)_3)\}_4Mo_4O_{16}]$ **2a**

$[\{Ru(\eta^6\text{-}C_6H_2(CH_3)_4)\}_4Mo_4O_{16}]$ **3a**

$[\{Ru(\eta^6\text{-}1,4\text{-}CH_3C_6H_4CH(CH_3)_2)\}_4Mo_4O_{16}]$ **4a**

Windmill isomers:

$[\{Ru(\eta^6\text{-}p\text{-}CH_3C_6H_4CH(CH_3)_2)\}_4Mo_4O_{16}]$ **4b**

$[\{Ru(\eta^6\text{-}C_6Me_6)\}_4Mo_4O_{16}]$ **5b**

$[\{Ru(\eta^6\text{-}C_6H_5CH_3)\}_4Mo_4O_{16}]$ **1b**

Spectroscopic characterization: The IR spectra of the triple-cubane complexes **1a**, **2a** and **3a** display the same absorption pattern, with two strong bands characteristic of *cis*-MoO_2 units (ν_{as} and ν_s modes) in the range of 900–930 cm^{-1}.[11] The Raman spectrum of solid **1a** (Figure 1) in this region also displays *cis*-MoO_2 ν_{as} and ν_s modes, at 905 (w) and 940 cm^{-1} (s). It is noteworthy that the classical reversal of relative band intensities is observed on changing from IR to Raman spectroscopy.[11a] By contrast, the IR and Raman spectra of the solid windmill-like complex **4b** exhibit a single broad band at about 920 cm^{-1}, characteristic of the $\nu(Mo{=}O_t)$ mode; $\nu(M\text{-}O_b\text{-}M)$ bands are observed in the range of 700–850 cm^{-1}. In this region, the triple-cubane complexes exhibit only one band in the IR (ca. 700 cm^{-1} for **1a**, **2a** and **3a**) and Raman spectra (790 cm^{-1} for **1a**), while the

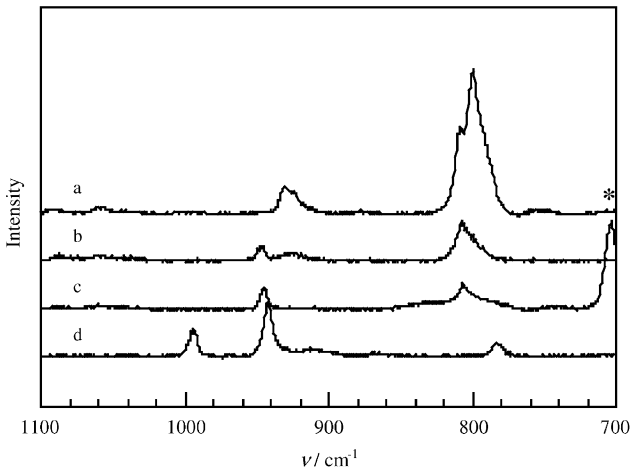

Figure 1. Raman spectra of solid-state samples of **1a** (d) and **4b** (a) and of solutions of **4b** in chloroform (b) and dichloromethane (c). *: attributed to the solvent.

IR and Raman spectra of the windmill-like complex **4b** display two very strong bands. All complexes **1a**, **1b**, **2a** and **3a** give rise to four groups of absorptions for the arene ligand, assigned to ν(CH) (above 2900 cm^{-1}), ν(CC) (1380–1525 cm^{-1}), δ(CH) (ca. 1030 cm^{-1}) and π(CH) (850–880 cm^{-1}). The other bands, below 700 cm^{-1}, are associated with the oxometal core.

Given the different spectral features of triple-cubane and windmill isomers, the solid obtained by refluxing **1a** in methanol can be easily recognized as a mixture of **1a** and **1b**. Indeed its infrared spectrum displays, besides the bands of **1a**, two ν(M-O_b-M) bands at 782 and 738 cm^{-1}.

Furthermore, the Raman spectrum of **4b** in chloroform or dichloromethane reveals the presence of the two isomers **4a** and **4b** and thus confirms the existence of an equilibrium in solution.[9a] However, the ratio of the two isomers cannot be determined precisely by analysis of Raman-band intensity because of their different absorption coefficients.

The ^{1}H NMR spectra of **1a** and **2a** in $CDCl_3$ indicate that all arene ligands are magnetically equivalent, which is consistent with the X-ray structures of the complexes. However, the ^{1}H NMR spectrum of the mixture of **1a** and **1b** displays only one set of signals in $CDCl_3$ solution; furthermore, these signals have the same chemical shifts as those observed for **1a** in $CDCl_3$. These observations are in agreement with the assumption of the presence of a single species in solution in the case of **1**. Finally, an EXAFS study of a solution of **1a** in $CHCl_3$ showed that the solid-state structure of **1a** is retained on dissolution in chlorinated solvents (see below).

Crystal structures: Compounds **1a**·7 H_2O, **2a**·5 H_2O and **3a**·2 CH_2Cl_2·2 H_2O were characterized by X-ray crystallography. Selected bond lengths are given in Table 1. The molecular structures of **1a**, **2a** and **3a** are displayed in Figure 2. The three clusters have a triple-cubane structures related to that of $[\{Rh^{III}Cp^*\}_4Mo_4O_{16}]$ ($Cp^* = \eta^5$-C_5Me_5), described by Isobe et al.[12] Their structure can be described as a linear assembly of two $[\{Ru(\eta^6\text{-arene})\}_2(MoO_3)_2(\mu_3\text{-}O)_4]^{4-}$ and one central $[(MoO_3)_4(\mu_3\text{-}O)_4]^{8-}$ cubes by face sharing. The triple-cubane clusters **1a**, **2a** and **3a** contain six-coordinate Mo centres displaying the classical two short (terminal oxo ligands), two medium and two long Mo–O distances typical of class II polyoxometalates,[13] while the Mo–O bond lengths in **4b** differ more widely, as shown in Table 2. It is noteworthy that, despite these differences, the average Mo–O bond lengths in **1a** and **4b** are similar (1.99(26) and 1.98(23) Å, respectively).

Table 1. Selected bond lengths [Å] for **1a**·7 H_2O, **2a**·5 H_2O, and **3a**·2 CH_2Cl_2·2 H_2O.

1a·7 H_2O					
Mo1–O10	1.70(1)	Mo1–O11	1.73(1)	Mo1–O12	1.944(9)
Mo1–O12′	2.324(9)	Mo1–O112	1.902(9)	Mo1–O1222	2.338(9)
Mo2–O12	2.38(1)	Mo2–O20	1.71(1)	Mo2–O21	1.72(1)
Mo2–O122′	1.916(9)	Mo2–O1222	1.930(8)	Mo2–O1222′	2.377(8)
Ru1–O12′	2.120(9)	Ru1–O112	2.08(1)	Ru1–O122	2.09(1)
Ru2–O112	2.11(1)	Ru2–O122	2.057(9)	Ru2–O1222	2.106(8)
2a·5 H_2O					
Mo1–O10	1.70(2)	Mo1–O11	1.71(2)	Mo1–O112	1.89(2)
Mo1–O1123	2.35(2)	Mo1–O1224	2.32(2)	Mo1–O13341.96(2)	
Mo2–O20	1.68(2)	Mo2–O21	1.68(2)	Mo2–O122	1.87(2)
Mo2–O1123	2.33(2)	Mo2–O1224	2.37(1)	Mo2–O2344	1.96(2)
Mo3–O30	1.65(2)	Mo3–O31	1.72(2)	Mo3–O334	1.92(2)
Mo3–O1123	1.94(1)	Mo3–O1334	2.34(1)	Mo3–O2344	2.36(2)
Mo4–O40	1.70(2)	Mo4–O41	1.68(2)	Mo4–O443	1.92(2)
Mo4–O1224	1.91(1	Mo4–O1334	2.36(2)	Mo4–O2344	2.33(2)
Ru1–O112	2.11(2)	Ru1–O122	2.11(2)	Ru1–O11232.11(2)	
Ru2–O112	2.11(2)	Ru2–O122	2.10(2)	Ru2–O1224	2.15(2)
Ru3–O334	2.11(2)	Ru3–O443	2.11(2)	Ru3–O1334	2.09(2)
Ru4–O334	2.10(2)	Ru4–O443	2.09(2)	Ru4–O2344	2.09(1)
3a·2 CH_2Cl_2·2 H_2O					
Mo1–O1	1.693(2)	Mo1–O6	1.918(2)	Mo1–O8	2.319(2)
Mo1–O2	1.706(2)	Mo1–O7	2.388(2)	Mo1–O8′	1.948(2)
Mo2–O8	2.379(2)	Mo2–O3	1.704(2)	Mo2–O7	2.318(2)
Mo2–O4	1.701(2)	Mo2–O5	1.921(2)	Mo2–O7′	1.943(2)
Ru1–O5	2.089(2)	Ru1–O6	2.114(2)	Ru1–O8	2.089(2)
Ru2–O7	2.096(2)	Ru2–O5	2.098(2)	Ru2–O6	2.098(2)

X-ray absorption spectra of 1a, 1b and 4b: Solid-state X-ray absorption spectra were recorded at room temperature for **1a** and **4b**, as well as for the mixture of **1a** and **1b** obtained by refluxing a suspension of **1a** in methanol. The extended X-ray absorption fine structure (EXAFS) signals of **1a** and **4b** were modelled by using the FEFF7 code[14] with

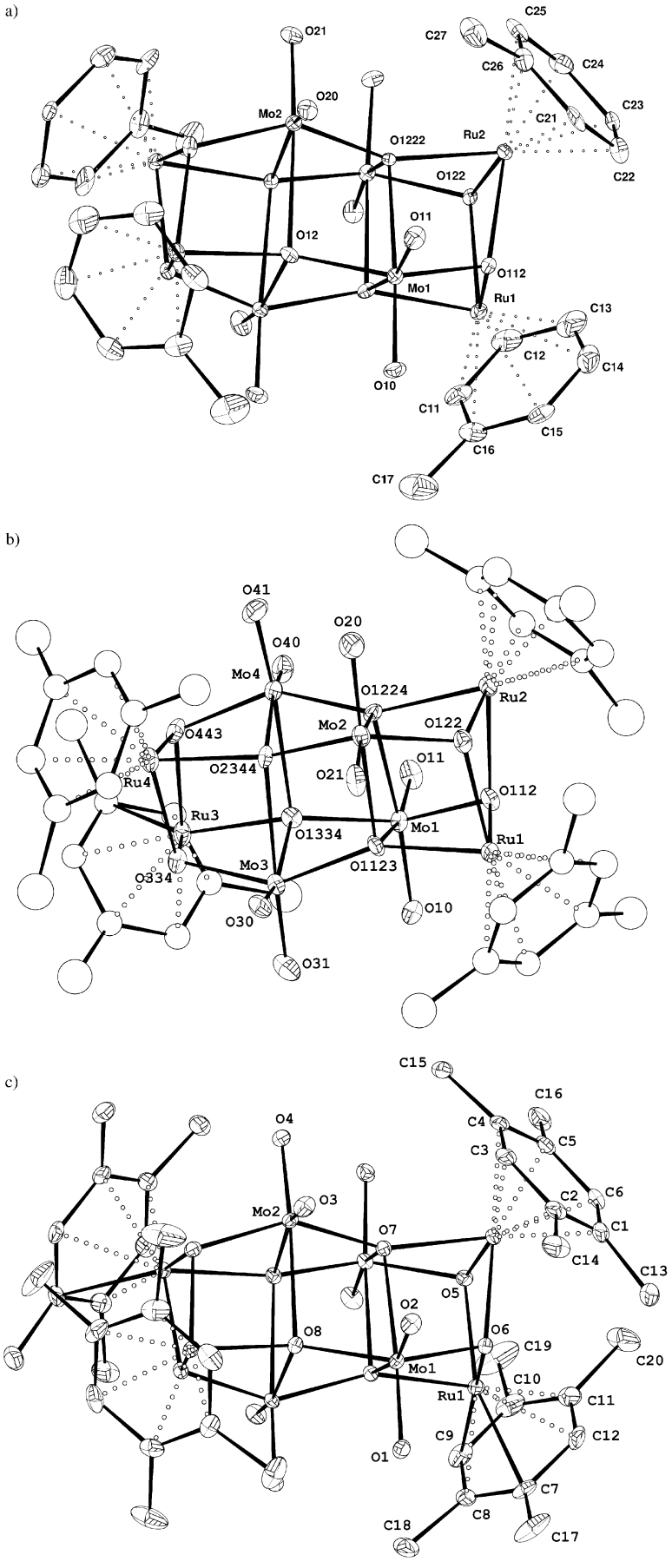

Figure 2. Molecular structures (20 % probability thermal ellipsoids) of **1a** (a), **2a** (b) and **3a** (c).

structural parameters derived from the single-crystal X-ray analyses. Figure 3 shows the modulus and the imaginary part of the Fourier transforms of the experimental and calculated EXAFS signals of **1a** and **4b** with inclusion of multiple scattering. The calculated FT spectra of **1a** and **4b** are in close agreement with the experimental data, and the assignment of the peaks is straightforward. The X-ray structure analyses showed that 1) in both cases the four Mo atoms are hexacoordinate with very similar average Mo–O bond lengths, but 2) the Mo–O distances lie in different ranges in the two compounds (Table 2). The Fourier transforms of the EXAFS signals of **1a** and **4b** indeed reflect these differences, since the first shell corresponding to the six nearest oxygen atoms consists of a single, large peak for **4b** but of three peaks for **1a**.

Given these differences, the EXAFS signal of the mixture of solid **1a** and **1b** was well fitted by a 50/50 combination of the EXAFS signals of **1a** and **4b** (Figure 4), the latter of which has a windmill-like structure identical to that of **1b**, with the exception of the arene ligands. This was confirmed by comparing the X-ray absorption near-edge structure (XANES) spectrum of the mixture to those of **1a** and **4b**. On the basis of these data, the solid containing **1a** and **1b** is proposed to be an equimolar mixture of the two isomers. This means that refluxing **1a** in methanol for at least 12 h did not convert the triple-cubane complex **1a** completely to the windmill isomer **1b**. An X-ray absorption study on a solution of **1a** in chlorofom was also performed, but in fluorescence mode due to the low solubility of **1a**. Despite the poor quality of the EXAFS signal obtained in fluorescence mode, the signals of **1a** in solution and in the solid state are rather sim-

Table 2. Typical Mo–O bond lengths [Å][a] for **1a** and **4b**.

1a	**4b**
1.70(1)	1.706(3)
1.73(1)	1.798(3)
1.902(9)	1.804(3)
1.944(9)	2.073(3)
2.324(9)	2.122(3)
2.338(9)	2.365(3)

[a] These distances correspond to the Mo–O bond lengths around one arbitrarily chosen Mo atom of each compound (Mo1 for **1a**·7 H_2O, and Mo1 for **4b**).

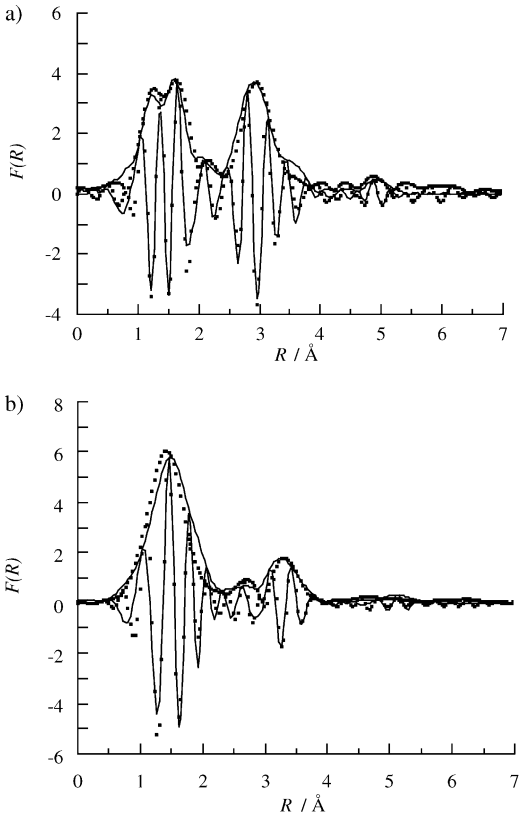

Figure 3. Modulus and imaginary part of the Fourier transforms of the experimental (dotted line) and calculated (full line) EXAFS signals of solid **1a** (a) and **4b** (b), including multiple scattering.

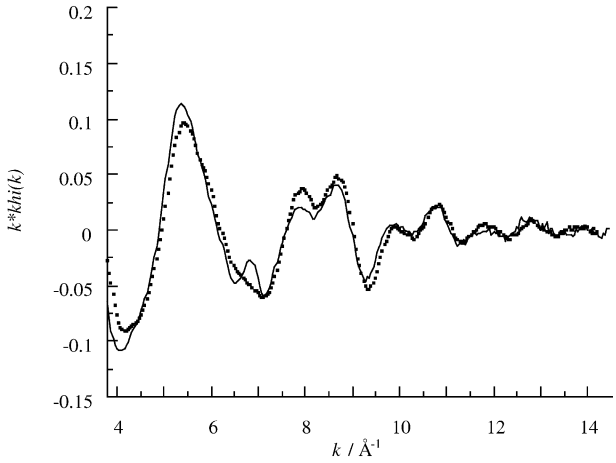

Figure 4. Experimental and simulated EXAFS signals of the mixture of solid **1a** and **1b**.

ilar, that is, the molecular structure of **1a** is essentially maintained in solution.

Finally, X-ray absorption spectra were recorded for solutions of **4b** in chloroform and dichloromethane. We proposed previously that **4b** exists in these solvents as a mixture of the two isomers: the windmill form and possibly the triple-cubane form.[9a] The present EXAFS study confirms the presence of the triple-cubane form and the existence of the equilibrium **4b**⇄**4a**. The EXAFS signals and the FT EXAFS signals of **4b** in dichloromethane or chloroform are indeed well fitted by a combination of the EXAFS signals of **4b** and **1a** in the solid state. The best fit was obtained for a ratio of triple-cubane to windmill isomer of 60/40 in chloroform (Figure 5a) and 80/20 in dichloromethane (Figure 5b). These values are in close agreement with the conclusion of the NMR study previously reported.[9a]

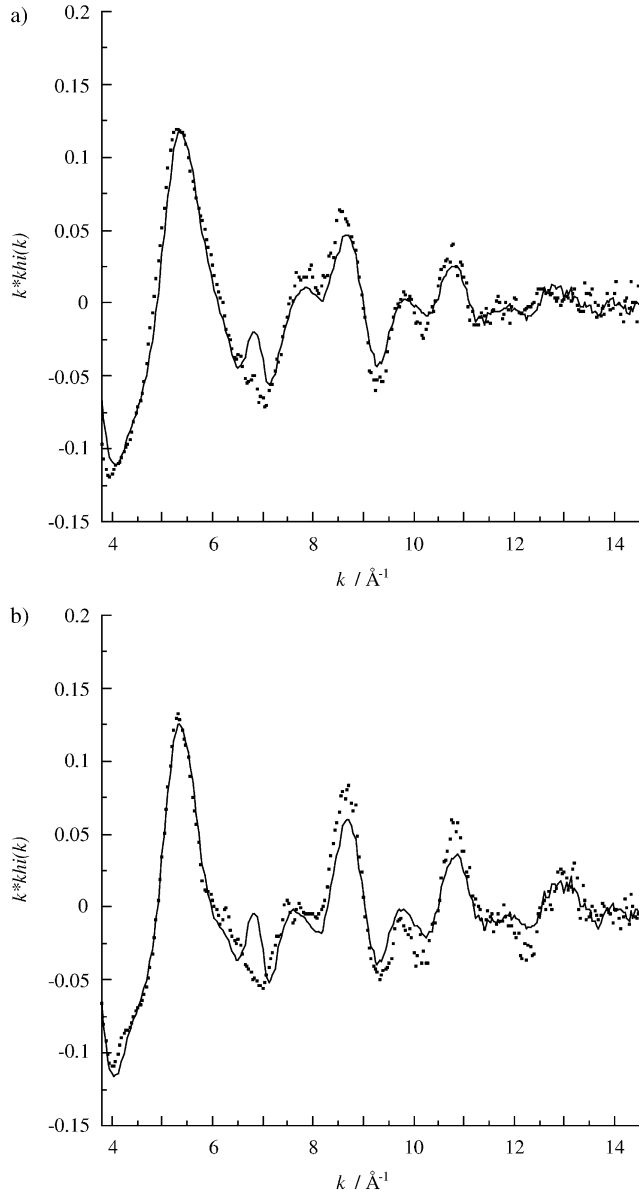

Figure 5. Experimental (dotted line) and simulated (full line) EXAFS signals of **4b** in solution in dichloromethane (a) and chloroform (b).

DFT calculations: DFT calculations and geometry optimisations were carried out on [{Ru(η^6-arene)}$_4$Mo$_4$O$_{16}$] molecules with various arene ligands (benzene, **6**; toluene, **1**; mesitylene, **2**; *p*-cymene, **4**; hexamethylbenzene, **5**) both for the triple-cubane (**a**) and windmill (**b**) isomers to investigate the role of the ligands in the relative stability of the isomers. The obtained metal–oxygen bond lengths, the nonbonding metal–metal distances and the distances from the Ru atoms to the centroid Ω of the arene ligands are listed in Table 3. The short metal–oxygen distances calculated for both types of isomers reproduce quite satisfactorily the parameters determined by X-ray analyses on **1a**, **2a** and **4b**[7] (Tables 1 and 2). However, the long Mo–O distances are overestimated by 0.15–0.20 Å. The variations in the Ru–Ω distance provide an interesting clue for the detection of steric hindrance originating in the arene substituents. This distance is remarkably invariant in the windmill isomers, in agreement with Ru···Ru distances that are large enough (>5.3 Å) to accommodate bulky arene ligands. The situation is different for the triple-cubanes, in which the shortest Ru···Ru distances lie between 3.32 and 3.42 Å (Table 3). For this isomer, the calculated Ru–Ω distance consistently increases with increasing size of the arene ligand (Table 3). However, the elongation Δ(Ru–Ω) calculated with respect to benzene remains less than 0.01 Å for all investigated arenes, except for C_6Me_6, for which Δ(Ru–Ω) is 0.028 Å. One can therefore expect the steric strain to become significant only for **5a**.

The relative energies calculated for both isomers along the series of five arene ligands are listed in Table 4. In all cases, the windmill form is most stable, and energy differences ΔE range from 9.1 kcal mol^{-1} for mesitylene to 18.6 kcal mol^{-1} for C_6Me_6. These results clearly indicate that an isolated molecule of [{Ru(η^6-arene)}$_4$Mo$_4$O$_{16}$] is intrinsically more stable in the windmill form. However, the relatively large range of ΔE suggests that the arene ligands contribute to the relative stability of the isomers. The $\Delta(\Delta E)$ value represents the variation of ΔE as a function of the arene ligand with respect to benzene. Though it is clear from Table 4 that no correlation can be found between $\Delta(\Delta E)$ and the bulk of the ligands, a finer structural analysis is needed. A difficulty encountered throughout this study is related to the multiplicity of the local minima associated with the various possible positions of partly substituted arenes. When no crystal structure was available, the starting geometry was chosen to minimize the arene···arene contacts. However, in some cases application of this criterion was ambiguous, especially with the *p*-cymene ligand. For **4a** and **4b**, two starting geometries were eventually retained and yielded distinct minima at the end of the optimization process.

For **4b**, the energy difference between the two minima was only 0.5 kcal mol^{-1}, but it amounted to 2.3 kcal mol^{-1} for **4a** (Table 4), a difference which is neither negligible nor interpretable in terms of steric hindrance. However, for the two forms of **4a**, as for the other investigated molecules, the

Table 4. Relative energy ΔE [kcal mol^{-1}], number of O···H contacts shorter than 3.5 Å calculated for **6b**, **6a**, **1b**, **1a**, **2b**, **2a**, **4b**, **4a**, **5b**, **5a**, and the difference Δ(O··H) in the number of such contacts between the windmill and triple-cubane forms. For **1a**, **2a**, **4a** and **5a**, $\Delta(\Delta E)$ represents the modification of the destabilization energy of the triple-cubane form with respect to the value calculated for benzene (**6a**).

	ΔE	O···H	Δ(O···H)	$\Delta(\Delta E)$	Δ[Δ(O···H)]
6b	0	28			
6a	+15.5	24	−4		
1b	0	32			
1a	+13.5	44	+12	−2.0	+16
2b	0	46			
2a	+9.1	56	+10	−6.4	+14
4b	0	40			
4b[a]	+0.5	40			
4a	+14.2	48	+8	−1.3	+12
4a[a]	+16.5	40	0	+1.0	+ 4
5b	0	54			
5a	+18.6	52	−2	+3.1	+2

[a] Two structures differing in the arene position were optimized for **4a** and **4b**.

Table 3. Selected bond lengths [Å] calculated for the windmill and the triple-cubane isomers of [{Ru(η^6-C_6H_6)}$_4$Mo$_4$O$_{16}$] (**6b**, **6a**), [{Ru(η^6-$C_6H_5CH_3$)}$_4$Mo$_4$O$_{16}$] (**1b**, **1a**), [{Ru(η^6-$C_6H_3(CH_3)_3$}$_4$Mo$_4$O$_{16}$] (**2b**, **2a**), [{Ru(η^6-1,4-$CH_3C_6H_4CH(CH_3)_2$}$_4$Mo$_4$O$_{16}$] (**4b**, **4a**), and [{Ru(η^6 $C_6(CH_3)_6$}$_4$Mo$_4$O$_{16}$] (**5b**, **5a**).

Distances	Position	**6b**	**1b**	**2b**	**4b**[a]	**5b**	**6a**	**1a**	**2a**	**4a**[a]	**5a**
Ru–O	μ-O(MoRu)	2.084	2.085	2.091	2.096/2.083	2.084					
		2.087	2.091	2.092	2.097/2.090	2.090					
Mo–O	μ-O(MoRu)	1.832	1.834	1.832	1.831/1.832	1.833					
		1.856	1.856	1.858	1.856/1.858	1.858					
Ru–O	μ_3-O(RuRuMo)						2.119	2.116	2.120	2.137/2.126	2.146
Mo–O	μ_3-O(RuRuMo)						1.986	1.980	1.974	1.975/1.977	1.966
Ru–O	μ_4-O(RuMoMoMo)	2.089	2.088	2.099	2.090/2.105	2.139	2.076	2.088	2.081	2.075/2.091	2.098
Mo–O	μ_4-O(RuMoMoMo)	2.066	2.062	2.052	2.056/2.060	2.050	1.948	1.946	1.934	1.944/1.946	1.958
		2.141	2.145	2.141	2.132/2.136	2.108					
		2.57	2.57	2.61	2.62/2.59	2.785	2.48	2.485	2.52	2.475/2.480	2.44
Mo–O	terminal	1.745	1.746	1.749	1.749/1.747	1.746	1.741	1.743	1.741	1.745/1.747	1.748
Ru···Mo		3.22	3.23	3.24	3.23/3.23	3.23	3.32	3.33	3.33	3.32/3.32	3.305
		3.35	3.35	3.37	3.36/3.36	3.41	3.90	3.92	3.91	3.89/3.92	3.94
M···Mo		3.40	3.40	3.38	3.37/3.39	3.33	3.46	3.47	3.49	3.46/3.46	3.445
		3.75	3.75	3.78	3.79/3.75	3.90	4.12	4.11	4.14	4.14/4.104.03	
Ru···Ru		5.40	5.41	5.42	5.39/5.43	5.38	3.326	3.325	3.33	3.361/3.347	3.42
		6.32	6.31	6.34	6.33/6.36	6.46					
Ru–Ω[b]		1.696	1.695	1.694	1.693/1.699	1.696	1.691	1.696	1.698	1.694/1.700	1.719

[a] Two structures differing in the orientation of the *p*-cymene ligand were calculated for this isomer. [b] Ω: centroid of the arene ring.

presence of relatively short (typically less than 3.5 Å) contacts between oxygen atoms of the $\{Ru_4Mo_4O_{16}\}$ core and hydrogen atoms of the arene ring and its substituents was found. Since these contacts are too long to generate steric strain, they can be assumed favorable due to electrostatic attraction. The number of such O···H contacts, the difference Δ(O····H) in the number of contacts between the triple-cubane and the windmill isomers and the variations of Δ(O····H) with the number of alkyl substituents on the arenes relative to benzene are listed in Table 4 for all investigated complexes. It appears that $\Delta[\Delta(O\cdots H)]$ is positive for all substituted arenes, that is, bulkier ligands approach the oxo core of triple-cubane isomers more closely than that of windmill isomers. With regard to energy, $\Delta(\Delta E)$ is negative for all substituted arenes, with the notable exception of C_6Me_6. For the complexes with toluene, mesitylene and *p*-cymene, the decrease in the relative stability of the windmill isomers with respect to $[\{Ru(\eta^6\text{-}C_6H_6)\}_4Mo_4O_{16}]$ thus displays a reasonable correlation with the larger increase in the number of O···H contacts in the triple-cubane isomer. Another interesting hint is provided by comparison of the ligand positions optimized for **4a** and **4b**. The two forms of the triple-cubane structure with *p*-cymene ligands differ in the number of O···H contacts ($\Delta(O\cdots H) = 8$ and 0; Table 4), and the form with the largest number of such contacts is calculated to be more stable by 2.3 kcal mol^{-1}. However, the number of O···H contacts is identical in the two forms calculated for the windmill structure, which differ in energy of by only 0.5 kcal mol^{-1} (Table 4).

Clearly, however, this correlation is not sufficient to explain the features of **5a**: the difference in the number of O····H contacts between the two isomers is very close to that obtained for benzene and does not explain the calculated $\Delta(\Delta E)$ value of $+3.1$ kcal mol^{-1} corresponding to an enhanced destabilization of the triple-cubane form (Table 4). This result should rather be interpreted as a consequence of the steric strain induced by C_6Me_6 in the triple-cubane isomer, evidenced by a significant elongation of the Ru–Ω distance (Table 3).

Conclusion

Two isomers corresponding to the general composition $[\{Ru(\eta^6\text{-arene})\}_4M_4O_{16}]$ have been recognized. They differ in the positions of the organometallic units around the central $\{M_4O_{16}\}$ core and are referred to as windmill and triple-cubane forms, whose connectivities can be described as $[\{Ru(\eta^6\text{-arene})\}_4\{MO\}_4(\mu\text{-}O)_8(\mu_4\text{-}O)_4]$ and $[\{Ru(\eta^6\text{-arene})\}_4\{MO_2\}_4(\mu_3\text{-}O)_4(\mu_4\text{-}O)_4]$, respectively. Up to now, only the windmill form had been characterized in the solid state, for $[\{Ru(\eta^6\text{-}1,4\text{-}CH_3C_6H_4CH(CH_3)_2)\}_4Mo_4O_{16}]$ (**4b**) and $[\{Ru(\eta^6\text{-}C_6Me_6)\}_4M_4O_{16}]$ (M = Mo, W). We thus report herein the first X-ray crystallographic characterization of {Ru(arene)}-containing triple-cubane organometallic oxides, namely, $[\{Ru(\eta^6\text{-}C_6H_5CH_3)\}_4Mo_4O_{16}]$ (**1a**), $[\{Ru(\eta^6\text{-}1,3,5\text{-}C_6H_3(CH_3)_3\}_4Mo_4O_{16}]$ (**2a**), and $[\{Ru(\eta^6\text{-}1,2,4,5\text{-}C_6H_2(CH_3)_4\}_4Mo_4O_{16}]$ (**3a**), obtained by reaction of the corresponding ruthenium dimer $[\{Ru(arene)Cl_2\}_2]$ with the molybdates $[MoO_4]^{2-}$ in water or with $[Mo_2O_7]^{2-}$ in organic solvents.

While characterizing $[\{Ru(\eta^6\text{-}1,4\text{-}CH_3C_6H_4CH(CH_3)_2)\}_4Mo_4O_{16}]$ (**4b**) in chlorinated solvents, we gained some evidence that its molecular structure, as determined in the solid state, is not maintained in solution, and we proposed that the windmill form is in equilibrium with its triple-cubane isomer. This assumption was in full agreement with a ^{17}O NMR study but needed further support. We report here that the existence of the triple-cubane isomer in solution is also suggested by Raman spectroscopy and corroborated by EXAFS spectroscopy at the Mo K-edge. Assuming that the environment of the Mo atoms should be only slightly affected by the nature of the arene ligand, solid samples of $[\{Ru(\eta^6\text{-}1,4\text{-}CH_3C_6H_4CH(CH_3)_2)\}_4Mo_4O_{16}]$ and $[\{Ru(\eta^6\text{-}C_6H_5CH_3)\}_4Mo_4O_{16}]$ provided us with models of the windmill and the triple-cubane isomers, respectively. Combinations of their solid-state EXAFS signals were used to model the EXAFS signal of **4b** in solution. Solutions in chloroform and dichloromethane were then found to correspond to a ratio of windmill to triple-cubane forms of 40/60 and 20/80, respectively. $[\{Ru(\eta^6\text{-}C_6H_5CH_3)\}_4Mo_4O_{16}]$ was also found to isomerize in methanol to give a mixture of windmill and triple-cubane isomers, as evidenced by IR and EXAFS spectroscopy in the solid state, while its EXAFS signals or that of the previous mixture recorded in chlorinated solvents are consistent with predominance of the windmill isomer. Such an equilibrium between the windmill and the triple-cubane isomers of $[\{RhCp^*\}_4W_4O_{16}]$ in solution was recently described by Isobe et al.[15]

The origin of the fluxionality in the $[\{Ru(\eta^6\text{-arene})\}_4M_4O_{16}]$ family was addressed by DFT calculations. Although the windmill isomer was found to be most stable, whatever the arene ligand, the fluxionality does not seem to have its origin in a small energy difference between both isomers, but rather in environmental effects. However, the role of O···H contacts between the oxo core and the hydrogen atoms of the arene ring was put forward to explain the decrease in the relative stability of the windmill isomer for $C_6H_5CH_3$, 1,3,5-$C_6H_3(CH_3)_3$ and 1,2,4,5-$C_6H_2(CH_3)_4$. It can be expected that the residual water present in most structures—with the notable exception of the windmill form of $[\{Ru(\eta^6\text{-}1,4\text{-}CH_3C_6H_4\text{-}CH(CH_3)_2)\}_4Mo_4O_{16}]$, reported by Süss-Fink et al.[7]—contributes to the stability of the crystal and possibly reduces or even reverses the energy gap between the the windmill and triple-cubane forms. The effect of association with water has not yet been investigated by calculations. However, the comparison between anhydrous $[\{Ru(\eta^6\text{-}1,4\text{-}CH_3C_6H_4CH(CH_3)_2)\}_4Mo_4O_{16}]$, characterized in the windmill form,[7] and the hydrated crystals reported here to contain the triple cubane suggests that the presence of water could favor formation of the latter species. This hypothesis is also substantiated by partial isomerization of hydrated **1a** to the windmill form in refluxing methanol. A conclusive test would be to structurally characterize **1**, **2** and **3** in an anhydrous environment, as was done for **4**.[7]

The result obtained on the isolated molecules could, however, help interpreting some experimental observations. For instance, $[\{Ru(\eta^6\text{-}C_6Me_6)\}_4Mo_4O_{16}]$, for which the calculated

energy gap is largest, presumably for steric reasons, always retains the windmill-type geometry in solution. On the contrary, the $\{Ru(\eta^6\text{-}1,4\text{-}CH_3C_6H_4CH(CH_3)_2)\}^{2+}$-containing cluster **4b** undergoes partial isomerization to the triple cubane in chlorinated solvents, and the $\{Ru(\eta^6\text{-}C_6H_5CH_3)\}^{2+}$-containing cluster **1a** also shows some isomerization in methanol.

Experimental Section

Materials: $(n\mathrm{Bu_4N})_2[Mo_2O_7]$ was prepared according to the literature procedure.[16] The synthesis of $[\{Ru(\eta^6\text{-}C_6H_5CH_3)Cl_2\}_2]$, $[\{Ru(\eta^6\text{-}1,3,5\text{-}C_6H_3(CH_3)_3)Cl_2\}_2]$, and $[\{Ru(\eta^6\text{-}1,2,4,5\text{-}C_6H_2(CH_3)_4)Cl_2\}_2]$ followed the general methods for preparation of $[\{Ru(arene)Cl_2\}_2]$ complexes.[17] Reagent-grade organic solvents (Acros organics, SDS and VWR international) and $Na_2MoO_4\cdot 2H_2O$ (Fluka or VWR international) were obtained from commercial sources and used as received.

Methods: IR spectra were recorded from KBr pellets on a Bio-Rad FT 165 or on a Perkin-Elmer FT IR 1720 X spectrometer. The Raman spectra were recorded on a double-monochromator Jobin-Yvon U1000 spectrophotometer equipped with a Coherent Ar^+ laser and a photon-counting detector. The ^{1}H NMR spectra were obtained with a Bruker AC 300 or a Varian Gemini 200 BB spectrometer. Elemental analyses were performed by the Analytical Service of Université Pierre et Marie Curie or by the Laboratoire de Chimie Pharmaceutique et Organique Propédeutique de L'Université de Genève.

Preparation of $[\{Ru(\eta^6\text{-}C_6H_5CH_3)\}_4Mo_4O_{16}]$ (1a): Method 1: $Na_2MoO_4\cdot 2H_2O$ (0.073 g, 0.30 mmol) was dissolved in water (5 mL). $[\{Ru(\eta^6\text{-}C_6H_5CH_3)Cl_2\}_2]$ (0.083 g, 0.15 mmol) was added, and the suspension was stirred at room temperature for 4 h. The unconverted $[\{Ru(\eta^6\text{-}C_6H_5CH_3)Cl_2\}_2]$ was then filtered off, and the solution was concentrated to dryness. The brown residue was extracted three times with 10 mL of $CHCl_3$. Evaporation of the solvent afforded a red powder. The most appropriate composition for this powder seems to be **1a**$\cdot 2H_2O$ according to elemental analysis. Crystals of composition **1a**$\cdot 7H_2O$ suitable for X-ray analysis were obtained by slow diffusion of toluene into a solution of **1a**$\cdot 2H_2O$ in $CHCl_3$. **1a**$\cdot 2H_2O$: Yield: 0.047 g (44 %). IR (KBr): $\tilde{\nu}$ = 3058 (w), 1443 (w), 1384 (w), 1037 (w), 931 (s), 905 (s), 853 (m), 706 (s), 653 (s), 621 (w), 585 cm^{-1} (m); ^{1}H NMR (300.13 MHz, $CDCl_3$, 22 °C, TMS): δ = 5.74 (t, 8 H, $C_6H_5CH_3$, ^3J = 5.7 Hz), 5.45 (t, 4 H, $C_6H_5CH_3$, ^3J = 5.4 Hz), 5.28 (d, 8 H, $C_6H_5CH_3$, ^3J = 5.8 Hz), 2.40 ppm (s, 12 H, $C_6H_5CH_3$); elemental analysis (%) calcd for $C_{28}H_{36}Mo_4O_{18}Ru_4$: C 23.22, H 2.50; found: C 23.19, H 2.84.

Method 2: A mixture of $(n\mathrm{Bu_4N})_2[Mo_2O_7]$ (0.394 g, 0.50 mmol) and $[\{Ru(\eta^6\text{-}C_6H_5CH_3)Cl_2\}_2]$ (0.132 g, 0.25 mmol) in CH_3CN (10 mL) was stirred at room temperature for 5 h. Red needles (0.050 g) were obtained by slow evaporation at room temperature of the orange-red solution after two days. These crystals appeared to decompose with loss of solvent. Nevertheless, a partial X-ray diffraction analysis confirmed the presence of the **1a** core but did not allow us to determine the number of CH_3CN molecules. Crystallographic data: triclinic, space group: $P\bar{1}$, a = 13.469(3), b = 16.414(3), c = 19.381(4) Å, α = 70.94(2), β = 77.26(2), γ = 89.24(2)°, V = 3942(2) Å^3. The IR spectrum of **1a**$\cdot x\,CH_3CN$ is essentially similar to that of **1a**$\cdot 2H_2O$, with the exception of the presence of bands attributed to acetonitrile, especially the ν_{CN} band at 2275 cm^{-1}.

Isomerization of $[\{Ru(\eta^6\text{-}C_6H_5CH_3)\}_4Mo_4O_{16}]$ (1a) in methanol: Compound **1a** (0.047 g) was added to methanol (10 mL). The suspension was refluxed for 2 h. The resulting orange solid was filtered and identified as a mixture of **1a** and **1b** by IR and X-ray absorption spectroscopy.

Preparation of $[\{Ru(\eta^6\text{–}1,3,5\text{-}C_6H_3(CH_3)_3)\}_4Mo_4O_{16}]$ (2a): Method 1: $Na_2MoO_4\cdot 2H_2O$ (0.082 g, 0.34 mmol) was dissolved in water (10 mL). $[\{Ru(\eta^6\text{-}1,3,5\text{-}C_6H_3(CH_3)_3)Cl_2\}_2]$ (0.100 g, 0.17 mmol) was added, and the suspension was stirred at room temperature for 15 h. Residual $[Ru(\eta^6\text{-}C_6H_3(CH_3)_3)Cl_2]_2$ was then filtered off, and the solution was evaporated to dryness. The brown residue was extracted with 10 mL of $CHCl_3$, and the red solution was layered with toluene. Small red-orange crystals of **2a** were obtained after four days (0.021 g, 15 %).

Method 2: A mixture of $(n\mathrm{Bu_4N})_2[Mo_2O_7]$ (0.252 g, 0.32 mmol) and $[\{Ru(\eta^6\text{-}1,3,5\text{-}C_6H_3(CH_3)_3)Cl_2\}_2]$ (0.093 g, 0.25 mmol) in CH_3CN (10 mL) was stirred at room temperature for 5 h. Residual $[\{Ru(\eta^6\text{-}1,3,5\text{-}C_6H_3(CH_3)_3)Cl_2\}_2]$ (0.016 g) was then filtered off. Red-orange crystals of **2a**$\cdot x\,CH_3CN$ were obtained after one week by slow evaporation at room temperature of the red solution (0.016 g, 8 % based on Ru). X-ray data: rhomboedral, $R3c$, a = 35.569(19), c = 21.802(6) Å, V = 23886(21) Å^3.

Method 3: A mixture of $(n\mathrm{Bu_4N})_2[Mo_2O_7]$ (0.252 g, 0.32 mmol) and $[Ru(\eta^6\text{-}1,3,5\text{-}C_6H_3(CH_3)_3)Cl_2]_2$ (0.093 g, 0.16 mmol) in MeOH (10 mL) was stirred at room temperature for 15 h. A brown precipitate, which has not been yet identified, was discarded, and the solution was allowed to stand at room temperature for a few days. Slow evaporation of the solvent afforded a mixture of yellow crystals of $(n\mathrm{Bu_4N})_2[Mo_6O_{19}]$ and red-orange crystals of **2a**. The mixture was dissolved in boiling acetone. Orange crystals of **2a**$\cdot 5H_2O$ suitable for X-ray analysis formed overnight (0.041 g, 32 % based on Ru). **2a**$\cdot 5H_2O$: IR (KBr), $\tilde{\nu}$ = 3074 (w), 2965 (w), 2919 (w), 1526 (m), 1444 (m), 1378 (m), 1303 (w), 1039 (m), 927 (s), 902 (s), 884 (m), 698 (s), 661 (s), 630 (s), 599 cm^{-1} (m); ^{1}H NMR (300 MHz, $CDCl_3$, 22 °C, TMS): δ = 4.86 (s, 12 H, $C_6H_3(CH_3)_3$), 2.39 ppm (s, 36 H, $C_6H_3(CH_3)_3$); elemental analysis (%) calcd for $C_{36}H_{58}Mo_4O_{21}Ru_4$: C 26.78, H 3.62 ; found: C, 27.12, H 3.69. The spectroscopic features (IR, ^{1}H NMR) of the products obtained by the three methods were identical.

Preparation of $[\{Ru(\eta^6\text{-}1,2,4,5\text{-}C_6H_2(CH_3)_4\}_4Mo_4O_{16}]$ (3a): $Na_2MoO_4\cdot 2H_2O$ (0.790 g, 3.26 mmol) was dissolved in 5 mL of water and added to an aqueous solution (20 mL) of $[\{Ru(\eta^6\text{-}1,2,4,5\text{-}C_6H_2(CH_3)_4)Cl_2\}_2]$ (0.200 g, 0.33 mmol). The suspension was stirred at room temperature for 4 h. The solvent was evaporated, and the product was extracted with dichloromethane (30 mL), then dried over $MgSO_4$. After evaporation of dichloromethane, **3a** was isolated (0.147 g; 57 % based on Ru). Orange crystals of **3a**$\cdot 2CH_2Cl_2\cdot 2H_2O$ suitable for X-ray analysis were obtained by slow diffusion of toluene into a solution of **3a** in dichloromethane. **3a**: IR (KBr), $\tilde{\nu}$ = 930 (s), 903 (s), 695 (m), 645 (s), 589 cm^{-1} (m); ^{1}H NMR (200 MHz, $CDCl_3$, 22 °C, TMS): δ = 5.21 (s, 8 H, $C_6H_2(CH_3)_4$), 2.25 ppm (s, 48 H, $C_6H_2(CH_3)_4$); elemental analysis (%) calcd for $C_{40}H_{56}Mo_4O_{16}Ru_4$: C 30.39, H 3.57; found: C, 30.21, H 3.71.

X-ray absorption studies: EXAFS measurements were performed at the Mo K-edge (19999 eV) on the XAS 13 beam line of the DCI storage ring at LURE (Orsay), operating at 1.85 GeV with an average ring current of 300 mA. The incident beam was monochromatized by a double Ge(400) crystal. The energy calibration was checked with an Mo foil reference. EXAFS spectra of solid samples of **1a**, **4b**, a mixture of **1a** and **1b** and solutions of **4b** were recorded in transmission mode by using argon-filled ionization chambers at room temperature. Each spectrum was acquired five (solid samples) or six times (solutions) with 2.5 eV steps and an integration time of 2 s per point. The solid samples were ground and homogeneously dispersed in cellulose pellets. The solutions of **4b** were studied by using a cell with a variable optical path adapted for XAS study. The solution of **1a** was studied in fluorescence mode with a seven-element solid detector by using a polychlorotrifluoroethylene cell. This spectrum was acquired twenty times with 2.5 eV steps and an integration time of 5 s per point.

The EXAFS data were analysed with the "EXAFS pour le Mac" package.[18] The EXAFS signal $k\chi(k)$ was extracted from the data by using a linear pre-edge background, a combination of polynomials and spline atomic absorption background and the normalisation procedure of Lengeler–Eisenberger.[19] The pseudoradial distribution functions are given by the Fourier transforms (FT) calculated on $w(k)k^3\chi(k)$, where $w(k)$ is a Kaiser–Bessel window with a smoothness parameter of 3. The k range was 2.6–15 Å^{-1} (Δk = 12.4 Å^{-1}). The FTs were calculated and presented without phase correction. The quality of the fits between the Fourier-filtered shells $k\chi_{exptl}(k)$ and the theoretical curve $k\chi_{theor}(k)$ was evaluated by an agreement factor ρ [%] equal to $\Sigma[k\chi_{exp}(k)-k\chi_{th}(k)]^2/\Sigma[k\chi_{exp}(k)]^2$. We used the FEFF7 code[14] to check for the presence of multiple scattering and to calculate the amplitude and phase functions $A_j(k,\pi)$ and $\phi_{i,j}(k)$ from model compounds (**1a** and **4b**).

Crystal structure analyses: Crystal structure data for **1a**$\cdot 7H_2O$, **2a**$\cdot 5H_2O$ and of **3a**$\cdot 2CH_2Cl_2\cdot 2H_2O$ are summarized in Table 5. Data for **1a**$\cdot 7H_2O$ and **2a**$\cdot 5H_2O$ were recorded at room temperature on an Enraf-Nonius CAD4 diffractometer, and for **3a**$\cdot 2CH_2Cl_2\cdot 2H_2O$ at 153 K on a Stoe Imaging Plate Diffraction System.[20] Crystals were mounted on glass

Table 5. Crystal structure data for **1a**·7 H_2O, **2a**·5 H_2O, and **3a**·2 CH_2Cl_2·2 H_2O.

	1a·7 H_2O	**2a**·5 H_2O	**3a**·2 CH_2Cl_2·2 H_2O
formula	$C_{28}H_{46}O_{23}Ru_4Mo_4$	$C_{36}H_{58}O_{21}Ru_4Mo_4$	$C_{42}H_{64}Cl_4Mo_4O_{18}Ru_4$
M_r	1538.7	1614.9	1786.8
color	red	red	orange
crystal system	monoclinic	trigonal	tetragonal
space group	*C*2/*c*	*R*3*c*	$I4_1/a$
T [K]	ambient	ambient	153
a [Å]	10.761(5)	35.801(14)	21.5456(10)
b [Å]	23.309(14)	35.801(20)	21.5456(10)
c [Å]	16.781(6)	21.933(7)	27.7407(14)
α [°]	90	90	90
β [°]	104.20(3)	90	90
γ [°]	90	120	90
V [Å^3]	4080(3)	24353(20)	12877.6(11)
Z	4	18	8
μ [cm^{-1}]	26.57	20.06	18.87
ρ_{calcd} [g cm^{-3}]	2.51	1.98	1.84
θ_{min}–θ_{max} [°]	1–25	1–25	2.24–25.97
decay of std. reflections [%]	7.66	<1	<1
reflections measured	3904	9977	24863
unique reflections (R_{int})	3594 (0.04)	4751 (0.067)	6236 (0.042)
obsd. reflections [$I>3\sigma(I)$]	1928	2513	5030 [$I>2\sigma(I)$]
absorption correction	ψ scan (min. 0.77, max. 1.00)	ψ scan (min. 0.69, max. 1.00)	DIFABS (min. 0.51, max. 0.85)
refined parameters	267	333	299
R[a]	0.053	0.051	0.026[b]
R_w	0.060[c]	0.057[c]	0.069[d]
weighting coefficients	4.08, −0.533, 5.98	16.2, −13.5, 12.2	0.0443[e]
GOF S	1.07	1.10	0.98
$\Delta\rho$ (max min^{-1}) [e.Å^{-3}]	1.30/−1.22	1.18/−1.22	0.57/−0.66

[a] $R=\Sigma||F_o|-|F_c||/\Sigma|F_o|$. [b] $R=\Sigma||F_o^2|-|F_c^2||/\Sigma|F_o^2|$. [c] $R_w=\Sigma w||F_o|-|F_c||^2/\Sigma w|F_o|^2$ ($w=w'[1-\{||F_o|-|F_c||/6\sigma(F_0)\}^2]^2$, where $w'=1/\Sigma_r A_R T_R(X)$ and $X=F_c/F_c$(max.) with three coefficients for a Chebyshev series. [d] $R_w=[\Sigma w(F_o^2-F_c^2)^2/\Sigma w(F_o)^4]^{1/2}$. [e] $w=1/[\sigma^2(F_o^2)+(0.0443P)^2]$, where $P=(F_o^2+2F_c^2)/3$.

fibers and sealed with an epoxy cement or by using a cryoloop (**3a**·2 CH_2Cl_2·2 H_2O). Reference reflections for **1a**·7 H_2O and **2a**·5 H_2O were periodically monitored for intensity and orientation control. Intensities were corrected for Lorentzian and polarization effects and for absorption (empirical).[21] For **1a**·7 H_2O and **2a**·5 H_2O, data processing and refinement were performed with the program CRYSTALS.[22] The structures were solved by direct methods and subsequent electron-density maps.[23] For **3a**·2 CH_2Cl_2·2 H_2O the structure was solved with SHELXS-97,[24] and weighted full-matrix least-squares refinement on F^2 (all reflections) was carried out with SHELXL-97.[25] All non-H atoms were refined anisotropically, except for **2a**·5 H_2O, for which only the metal and oxygen atoms were refined anisotropically, except for solvent molecules. Hydrogen atoms were not included in the refinements, except for **3a**·2 CH_2Cl_2·2 H_2O, for which they were included in calculated positions and treated as riding atoms by using default SHELXL parameters. Neutral-atom scattering factors were used, and anomalous dispersion correction was applied. Molecular structures of **1a**, **2a** and **3a** were drawn with the program CAMERON[26] (Figure 2). The asymmetric unit of **1a**·7 H_2O contains one "{{Ru(η^6-$C_6H_5CH_3$)}$_2$$Mo_2O_8$}" half-molecule and four molecules of water, one of which is in a special position. Molecules of **1a** are located on axis 2. The asymmetric unit of **2a**·5 H_2O contains one molecule and five molecules of water, all in general positions. The asymmetric unit of **3a**·2 CH_2Cl_2·2 H_2O contains one "{{Ru(η^6-1,2,4,5-$C_6H_2(CH_3)_4$)}$_2$$Mo_2O_8$}" half-molecule located at an inversion centre, and was estimated to contain one molecule of water and one molecule of dichloromethane (highly disordered), after modification of the reflection data file with the SQUEEZE routine in PLATON.[27]

CCDC-204526, CCDC-204527, and CCDC-205921 contain the supplementary crystallographic data for this paper. These data can be obtained free of charge via www.ccdc.cam.ac.uk/conts/retrieving.html (or from the Cambridge Crystallographic Data Centre, 12 Union Road, Cambridge CB21EZ, UK; fax: (+44) 1223-336-033; or deposit@ccdc.cam.uk).

Methods of calculation: All calculations were carried out with the formalism of the density functional theory (DFT) within the generalized gradient approximation (GGA), as implemented in the ADF program.[28] This formalism is based on the local spin-density approximation characterized by the electron-gas exchange ($X\alpha$ with $\alpha=2/3$) together with Vosko–Wilk–Nusair[29] parametrization for correlation. Nonlocal corrections due to Becke for the exchange energy[30] and to Perdew for the correlation energy[31] were added. For first-row atoms, the 1s shell was frozen and described by a single Slater function. The frozen core of the Mo and Ru atoms composed of the 1s to 3sp shells was also modelled by a minimal Slater basis. For hydrogen, carbon and oxygen, the Slater basis set used for the valence shell was of triple-ζ quality, supplemented with one p- or d-type polarization function.[32] The 4s and 4p shells of metal atoms were described by a double-ζ Slater basis, the 4d and 5 s shells by a triple-ζ basis and the 5p shell by a single orbital. No polarization function was added for metal atoms. Molecular bonding energies are reported with respect to an assembly of neutral atoms assumed to be isolated and in their ground state. Starting geometries were deduced from crystal structures, when available, or adapted to minimize the ligand···ligand contacts. The point groups corresponding to the maximal symmetry for an isolated molecule are S_4 for the windmill forms and D_{2d} for the triple-cubane isomers. Since the S_4 point group is not supported by ADF, all calculations on the windmill isomers were carried out with the constraints of the C_2 subgroup. For the sake of consistency, most calculations on the triple-cubane forms were carried out with the same constraints. However, the geometries eventually obtained at the end of the process exhibited little deviation with respect to the optimal symmetry. The geometry optimization processes were carried out by minimizing the energy gradient by the BFGS formalism[33] combined with a DIIS-type convergence acceleration method.[34] The optimization cycles were continued until all of the three following convergence criteria were fulfilled: 1) the difference in the total energy between two successive cycles was less than 0.001 hartree; 2) the difference in the norm of the gradient between two successive cycles was less than 0.001 hartree Å^{-1}; 3) the maximal difference in the Cartesian coordinates between two successive cycles was less than 0.01 Å.

[1] a) M. A. Bennett, T.-N. Huang, T. W. Turney, *J. Chem. Soc. Chem. Commun.* **1979**, 312; b) L. Plasseraud, G. Süss-Fink, *J. Organomet. Chem.* **1997**, *539*, 163; c) E. Garcia Fidalgo, L. Plasseraud, G. Süss-Fink, *J. Mol. Catal. A* **1998**, *132*, 5; d) M. Faure, A. Tesuro Vallina, H. Stoeckli-Evans, G. Süss-Fink, *J. Organomet. Chem.* **2001**, *621*, 103; e) G. Süss-Fink, M. Faure, T. R. Ward, *Angew. Chem.* **2002**, *114*, 105; *Angew. Chem. Int. Ed.* **2002**, *41*, 99f) G. Süss-Fink in *Synthetic Methods of Organometallic and Inorganic Chemistry, Vol. 10* (Ed.: W. A. Hermann), Georg Thieme, Stuttgart, **2001**.

[2] M. Bonchio, G. Scorrano, P. Toniolo, A. Proust, V. Artero, V. Conte, *Adv. Synth. Catal.* **2002**, *344*, 841.

[3] a) R. Jaouhari, P. Guenot, P. H. Dixneuf, *J. Chem. Soc. Chem. Commun.* **1986**, 1255; b) A. Fürstner, M. Liebl, C. W. Lehmann, M. Picquet, R. Kunz, C. Bruneau, D. Touchard, P. H. Dixneuf, *Chem. Eur. J.* **2000**, *6*, 1847; c) R. H. Grubbs, S. Chang, *Tetrahedron* **1998**, *54*, 4413; d) D. Jan, L. Delaude, F. Simal, A. Demonceau, A. F. Noels, *J. Organomet. Chem.* **2000**, *606*, 55.

[4] a) R. Mahé, Y. Sasaki, C. Bruneau, P. H. Dixneuf, *J. Org. Chem* **1989**, *54*, 1518; b) C. Ruppin, P. H. Dixneuf, S. Lécolier, *Tetrahedron Lett.* **1988**, *29*, 5365; c) K. Philippot, D. Devanne, P. H. Dixneuf, *J. Chem. Soc Chem. Commun.* **1990**, 1199; d) Y. Kita, H. Maeda, K. Omori, T. Okuno, Y. Tamura, *Synlett* **1993**, 273.

[5] T. Naota, H. Takaya, S.-I. Murahashi, *Chem. Rev.* **1998**, *98*, 2599.

[6] D. J. Edlund, R. J. Saxton, D. K. Lyon, R. G. Finke, *Organometallics* **1988**, *7*, 1692.

[7] G. Süss-Fink, L. Plasseraud, V. Ferrand, H. Stoeckli-Evans, *Chem. Commun.* **1997**, 1657.

[8] a) G. Süss-Fink, L. Plasseraud, V. Ferrand, S. Stanislas, A. Neels, H. Stoeckli-Evans, *Polyhedron* **1998**, *17*, 2817; b) L. Plasseraud, H. Stoeckli-Evans, G. Süss-Fink, *Inorg. Chem. Commun.* **1999**, *2*, 344.

[9] a) V. Artero, A. Proust, P. Herson, R. Thouvenot, P. Gouzerh, *Chem. Commun.* **2000**, 883; b) V. Artero, A. Proust, P. Herson, P. Gouzerh, *Chem. Eur. J.* **2001**, *7*, 3901; c) R. Villanneau, V. Artero, D. Laurencin, P. Herson, A. Proust, P. Gouzerh, *J. Mol. Struct.* **2003**, *656*, 67.

[10] H. Kang, S. Liu, S. N. Shaikh, T. Nicholson, J. Zubieta, *Inorg. Chem.* **1989**, *28*, 920.

[11] a) F. A. Cotton, R. M. Wing, *Inorg. Chem.* **1965**, *4*, 867; b) W. P. Griffith, J. D. Wickins, *J. Chem. Soc. A* **1968**, 400; c) F. W. Moore, R. E. Rice, *Inorg. Chem.* **1968**, *7*, 2510.

[12] Y. Hayashi, K. Toriumi, K. Isobe, *J. Am. Chem. Soc.* **1988**, *110*, 3666.

[13] M. T. Pope, *Hetero and Isopolyanions*, Springer, Berlin, New York, **1983**.

[14] S. I. Zabinsky, J. J. Rehr, J. J. Ankudinov, R. C. Albers, M. J. Eller, *Phys. Rev. B* **1995**, *52*, 2995.

[15] K. Nishikawa, K. Kido, J. Yoshida, T. Nishioka, I. Kinoshita, B. K. Breedlove, Y. Hayashi, A. Uehara, K. Isobe, *Appl. Organomet. Chem.* **2003**, *17*, 446.

[16] N. H. Hur, W. G. Klemperer, R.-C. Wang, *Inorg. Synth.* **1990**, *27*, 79.

[17] M. A. Bennett, A. K. Smith, *J. Chem. Soc. Dalton Trans.* **1974**, 233. M. A. Bennett, T. N. Huang, T. W. Matheson, A. K. Smith, *Inorg. Synth.* **1982**, *21*, 74.

[18] A. Michalowitz, EXAFS pour le MAC, Logiciels pour la chimie, Ed. Société Française de Chimie, Paris, **1991**.

[19] B. Lengeler, P. Eisenberger, *Phys. Rev. B* **1980**, *21*, 4507.

[20] Stoe Cie, *IPDS Software*, Stoe & Cie GmbH, Darmstadt, **2000**.

[21] N. Walker, D. Stuart, *Acta Crystallogr. Sect. A* **1983**, *39*, 158.

[22] D. J. Watkin, J. R. Carruthers, P. W. Betteridge, CRYSTALS, Chemical Crystallography Laboratory, University of Oxford, Oxford, **1996**.

[23] G. M. Sheldrick, SHELXS 86, Program for the solution of crystal structures, Universität Göttingen, Göttingen, **1986**.

[24] G. M. Sheldrick, SHELXS:97, Program for crystal structure determination, *Acta Crystallogr. Sect. A* **1990**, *46*, 467.

[25] G. Sheldrick, SHELXL 97, Universität Göttingen, Göttingen, Germany **1999**.

[26] L. J. Pearce, D. J. Watkin, CAMERON, Chemical Crystallography Laboratory, University of Oxford, Oxford, **1996**.

[27] A. L. Spek, PLATON/PLUTON version Jan. **1999**, *Acta Crystallogr. Sect. A* **1990**, *46*, 34.

[28] a) ADF User's Guide, Release **1999**, Chemistry Department, Vrije Universiteit, Amsterdam, The Netherlands, **1999**; b) E. J. Baerends, D. E. Ellis, P. Ros, *Chem. Phys.* **1973**, *2*, 41; c) G. te Velde, E. J. Baerends, *J. Comput. Phys.* **1992**, *99*, 84; d) C. Fonseca-Guerra, O. Visser, J. G. Snijders, G. te Velde, E. J. Baerends in *Methods and Techniques in Computational Chemistry, METECC-95* (Eds.: E. Clementi, G. Corongiu, STEF, Cagliari, Italy, **1995**, pp. 305–395.

[29] S. H. Vosko, L. Wilk, M. Nusair, *Can. J. Phys.* **1980**, *58*, 1200–1211.

[30] a) A. D. Becke, *J. Chem. Phys.* **1986**, *84*, 4524; b) A. D. Becke, *Phys. Rev. A.* **1988**, *38*, 3098.

[31] J. P. Perdew, *Phys. Rev. B.* **1986**, *33*, 8822–8824.

[32] J. G. Snijders, E. J. Baerends, P. Vernooijs, *At. Data Nucl. Data Tables* **1983**, *26*, 483; P. Vernooijs, J. G. Snijders, E. J. Baerends, Slater type basis functions for the whole periodic system, Internal Report, Free University of Amsterdam, The Netherlands, **1981**.

[33] T. H. Fisher, J. Almlöf, *J. Phys. Chem.* **1992**, *96*, 9768.

[34] L. Versluis, Ph.D. Thesis, University of Calgary, Calgary, Alberta, Canada, **1989**.

Received: July 25, 2003